Computer simulation of the SWI protocol in nuclear magnetic resonance imaging

Grzegorz Izydorczyk and Artur Klepaczko

Lodz University of Technology, Institute of Electronics
90-924 Lodz, ul. Wolczanska 211/215
izydorczyk.grzegorz@gmail.com, aklepaczko@p.lodz.pl

Abstract. In this paper a design of a computer simulator of susceptibility weighted imaging (SWI) protocol is presented. The ultimate application of the proposed system is to provide a framework for quantitative validation of SWI image processing algorithms. SWI is based on field non-uniformity caused by local susceptibility distribution and thus resulting in both measured signal phase shift and faster decay of transverse magnetization vector. The designed system accounts for both of these effects. Obtained simulated images demonstrate correctness of the results for simple objects, proving the propriety of the model.

1 Introduction

Magnetic resonance imaging (MRI) is currently a key diagnostic technology allowing for non-invasive visualization of soft tissues inside a human body. Within the MRI setting, susceptibility weighted imaging (SWI) is a relatively new concept [1] with the major application in venography. SWI is based on the effect of susceptibility-driven magnetic field perturbations leading to both – MR signal phase and magnitude local alterations. The current challanges in SWI processing embrace vein segmentation and detection of anomalies in the vessel system [2].

However, medical image processing methods require validation, i.e. evaluation of their accuracy and potential limits. Unfortunately, maintenance and operation of the MRI equipment is expensive and thus hardly available for experiments. In consequence, acquisition of real test images e.g. with the use of phantoms is significantly hampered. This brings a need for computer simulation which allows quantitative comparison of the processing results with the underlying ground-truth models. The described system enables formation of synthetic SWI images and as such it provides a framework for validation of SWI processing algorithms.

Since 1984, when the first one-dimensional MRI simulator was designed [3], a multiple of different approaches has been introduced [4–8]. Acceleration of processor clocks brought new possibilities to simulate with both higher precision and resolution. However only a few simulators account for magnetic field perturbations, allowing for susceptibility weighted imaging protocol simulation. The one suggested by Yoder [5] involved magnetic field inhomogeneities in numerical calculation of magnetization vector evolution by implementation of convolution

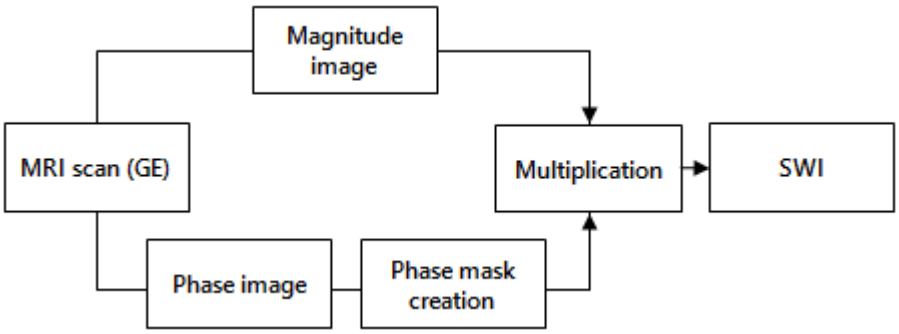

Fig. 1. SWI protocol data flow.

kernel. Later proposed SIMRI [6] implemented discrete time solution of Bloch equation and allowed for handling different field inhomogeneities along with T2* effects of Lorentz distribution. Yet another one, JEMRIS [7] solves the problem numerically, based on its mathematical description, thus leading to more accurate results, especially in case of time varying systems.

Proposed simulator, based on the SIMRI solution, estimates magnetic field perturbations induced by known geometries, thus making it dedicated for SWI.

2 Materials and methods

2.1 Susceptibility Weighted Imaging

The SWI protocol (Fig. 1) begins with typical Gradient Echo (GE) sequence, which results in complex signal consisting of magnitude and phase components [9]. The latter one is usually biased with phase wraps and strong nonlinearities around tissue boundaries, making post-processing unavoidable [10]. High-pass filtered phase values are then transformed into the range [0,1] according to a chosen map function, e.g. negative (eq. 1) or triangular (eq. 2) mask:

$$f(\boldsymbol{r}) = \begin{cases} \frac{\pi+\varphi(\boldsymbol{r})}{\pi} & -\pi < \varphi(\boldsymbol{r}) < 0 \\ 1 & 0 \leq \varphi(\boldsymbol{r}) < \pi \end{cases} \tag{1}$$

$$f(\boldsymbol{r}) = \begin{cases} \frac{\pi+\varphi(\boldsymbol{r})}{\pi} & -\pi < \varphi(\boldsymbol{r}) < 0 \\ \frac{\pi-\varphi(\boldsymbol{r})}{\pi} & 0 \leq \varphi(\boldsymbol{r}) < \pi \end{cases} \tag{2}$$

Received weights are finally used to decrease brightness of corresponding voxels in magnitude image. As a result, an image of enhanced tissue contrast is obtained thanks to phase jump on varying tissues boundaries.

2.2 MRI simulation

The designed simulator implements a 3D spoiled gradient echo sequence using a discrete time solution of Bloch equation, as described in [11]. It is assumed

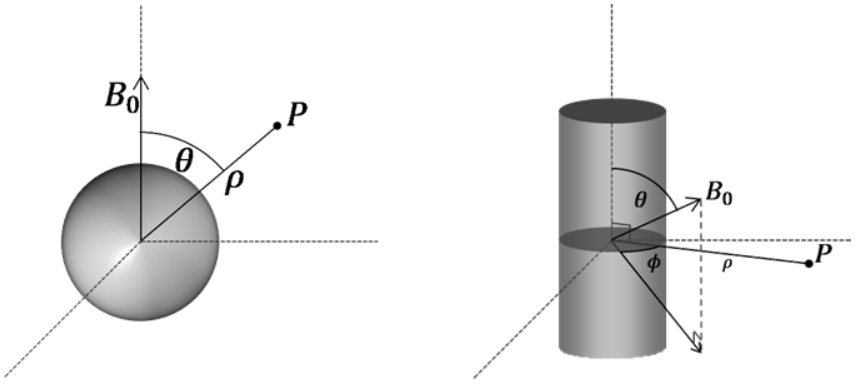

Fig. 2. Models of a sphere and long cylinder, both of radius R.

that the flow is fully compensated and thus it does not introduce additional phase errors. Evolution of magnetization vector $\boldsymbol{M}$ in position $\boldsymbol{r}$ at time $t + \Delta t$ can be expressed as a product of previous magnetization value, rotation matrix corresponding to spin precession $\mathbf{R}_{\text{prec}}$ and matrix of relaxation factors $\mathbf{R}_{\text{relax}}$ (eq. 3), both being a function of magnetic field perturbations $\Delta B(\boldsymbol{r})$.

$$\boldsymbol{M}(\boldsymbol{r}, t + \Delta t) = \boldsymbol{M}(\boldsymbol{r}, t)\mathbf{R}_{\text{prec}}(\boldsymbol{r})\mathbf{R}_{\text{relax}}(\boldsymbol{r}) \tag{3}$$

The time-independent perturbations are assumed to result from magnetic susceptibility alone. For known echo time (TE) parameter of GE sequence, phase component of the MRI signal $\varphi(\boldsymbol{r})$ can be estimated according to

$$\varphi(\boldsymbol{r}) = \gamma \Delta B(\boldsymbol{r}) TE. \tag{4}$$

In case of simple geometries such as sphere or long cylinder (Fig.2), which can model a tumor or a venous vessel, respectively, magnetic field perturbations can be evaluated analytically (eq. 5 and 6).

$$\Delta B(\rho) = \begin{cases} 0 & \rho < R \\ \frac{\Delta\chi}{3} B_0 \frac{R^3}{\rho^3}(3\cos^2\theta - 1) & \rho > R \end{cases}, \tag{5}$$

$$\Delta B(\rho) = \begin{cases} \frac{\Delta\chi}{6} B_0 (3\cos^2\theta - 1) & \rho < R \\ \frac{\Delta\chi}{2} B_0 \frac{R^2}{\rho^2} \sin^2\theta \cos 2\phi & \rho > R \end{cases}, \tag{6}$$

where ρ is the distance from the center of a sphere or the long axis of a cylinder, respectively, while angles θ and ϕ are defined as indicated in the Fig. 2.

In GE based sequences, spins at echo time do not rephase completely and as a result transverse component of magnetization vector decays faster, what is known as T2* effect. If a given voxel consists of N subvoxels, each described with magnetic field perturbations $\Delta B_i'$ and average perturbation over the voxel is

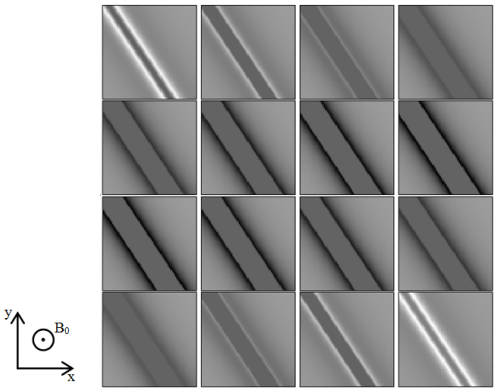

Fig. 3. Magnetic susceptibility driven field perturbations around a long cylinder in each slice along Z axis.

ΔB, additional signal decay $d(t)$ caused by intravoxel magnetization differences can be expressed by

$$d(t) \cong d(TE) = \frac{1}{N}\sqrt{\left(\sum_i \cos\vartheta_i\right)^2 + \left(\sum_i \sin\vartheta_i\right)^2} \tag{7}$$

where ϑ_i corresponds to the additional phase shift and is equal to

$$\vartheta_i = \gamma(\Delta B_i' - \Delta B)TE. \tag{8}$$

3 Results

In order to verify operation, several structures of well-defined susceptibility distribution were taken into consideration, modeled with real-life properties and tested under typical SWI sequence parameters (3 T, $TE = 17$ ms, $TR = 46$ ms, $FA = 10^\circ$), i.e. muscular venous vessel of 4 mm diameter and a spherical blood carrying tumor of 100 μm radius. Applied relaxation rates and proton density parameters are collected in Table 1.

3.1 Muscular venous vessel

Simulation was performed with cubic voxels of size $0.25\times0.25\times0.25$ mm, whereas magnetic field perturbations were approximated using eight times denser mesh in each direction, corresponding to averaging over 512 samples.

Distribution of magnetic field perturbations depicted in Fig. 3 follows the equation (5), providing clearly visible darker area inside the vein and influencing the surroundings in a complex manner. Depending on the orientation, local

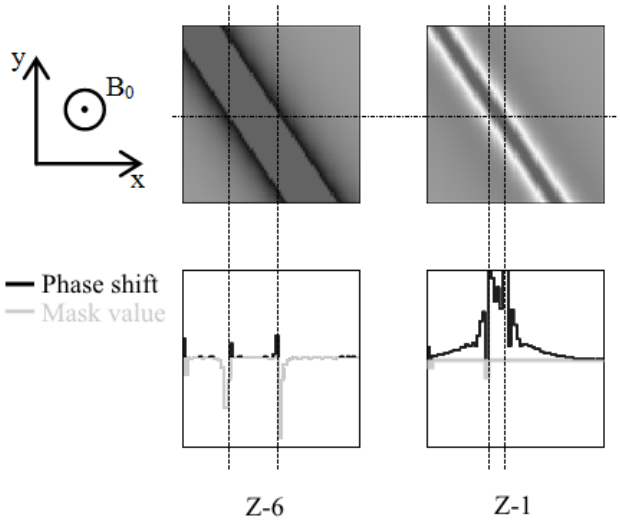

Fig. 4. Phase values with corresponding mask profiles gathered along X axis for two slices along B_0 direction and passing through the center of a voxel.

differences in magnetic field can be either negative (dark pixels) in the plane perpendicular to direction of the main magnetic field or positive (bright pixels) in the plane containing main magnetic field vector.

Applied homodyne-based high-pass filtering resulted in successful suppression of phase gradients in case of central slices but failed close to the field boundaries. Nonetheless, even with imperfect filtration it was possible to minimize gradient artifacts with the aid of negative mask function (Fig. 4).

Comparison of the number of mask multiplications indicates remarkable improvement of contrast between venous vessel and the surroundings (see Fig. 5), clearly exposing vessel walls. With further increase of the number of multiplications, contrast becomes stronger leading to overestimation of vessel dimensions and fake wall inside the venous vessel close to the region boundary. Four multiplications provided visually the best trade-off between contrast and distortions.

Table 1. Relaxation rates and proton density (PD) parameters

Tissue	1.5 T		3 T		PD
	T1 [ms]	T2 [ms]	T1 [ms]	T2 [ms]	[a.u.]
Muscle	1130	35	1420	33	79
Venous vessel	1440	122	1930	32	72
Gray matter	1124	95	1820	99	70

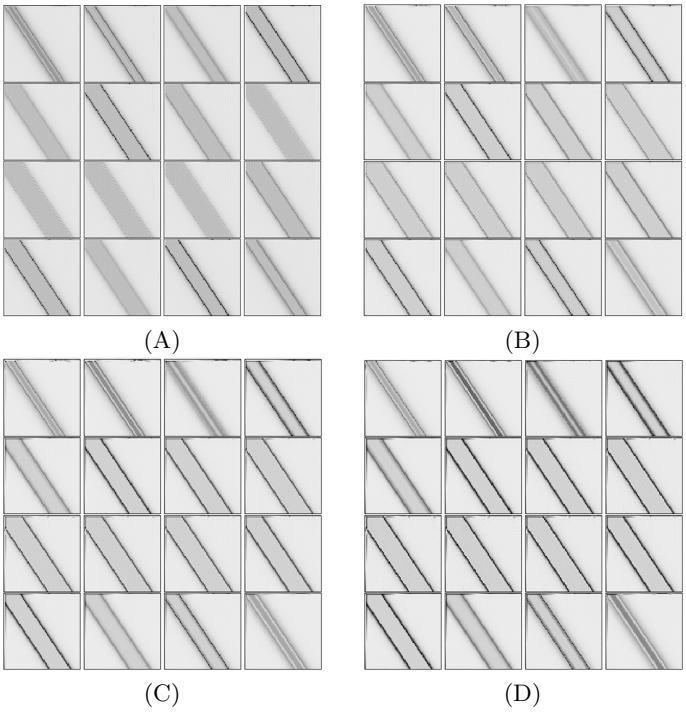

Fig. 5. Comparison of images using gradient echo (A) and SWI protocols: using 4 (B), 8 (C) and 16 (D) multiplications.

3.2 Brain blood carrying tumor

Another structure of well defined influence on magnetic field distribution is sphere, which can be used to model blood carrying tumor. In this case simulation was performed for $0.125 \times 0.125 \times 0.125$ mm voxel size, whereas magnetic field perturbations were estimated over 512 samples per voxel, as in the previous case. MRI signal has been biased with Gaussian noise of standard deviation of $\sigma = 1.2 \cdot 10^{-3}$ in each channel separately. Despite tiny dimensions of the investigated object and no perturbations inside of it, the sphere is clearly visible itself due to the external field alterations, being both negative in the plane perpendicular to the direction of main magnetic field and positive in the plain containing vector of main magnetic field (Fig. 6).

During phase image post-processing triangular mask was applied. This allowed to enhance contrast on the basis of both positive and negative phase shifts, resulting in almost uniform dark interior of a tumor. In order to remove noise, before further processing both magnitude and phase components were processed with 3×3 median filter for each slice. As a result (Fig. 7), strong blurring of the magnitude image can be noticed, whereas the phase one remains almost intact,

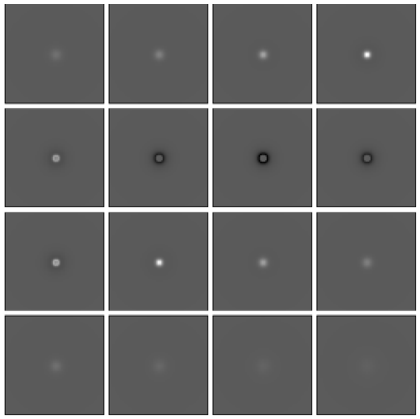

Fig. 6. Magnetic susceptibility driven magnetic field perturbations around a blood carrying tumor (sphere) in each slice along Z axis.

allowing for noise removal without losing phase information, hence the great benefit of susceptibility weighted imaging technique.

4 Summary

The proposed system allows for SWI protocol simulation. It accounts for local field perturbations due to the susceptibility distribution and takes advantage of subvoxel field estimation to evaluate faster signal decay known as T2* relaxation.

Visual resemblance of synthetic images comprising known geometries indicates correctness of the obtained results. However, a comparison between the real phantom and the outcome of proposed simulator of some simple object should be evaluated in order to verify its operation.

Intravoxel field perturbations introduce explicit difference into an MR image. Phase shifts on tissue boundaries leads to the enhancement of the image contrast. Moreover, as susceptibility driven magnetic field perturbations occur not only in space occupied by an object but also in its surroundings, SWI technique allows to reveal tiny structures, even of subvoxel dimensions. Therefore, simulation of susceptibility based effects should cover perturbations not only on the voxel- but also subvoxel-level. The proposed algorithm of T2* effect estimation is based on the assumption that magnetization vector after RF pulse is approximately constant over the voxel, which is not true when strong field perturbations are present inside of it. Under such circumstances, evolution of magnetization vector evaluated over denser grid than it comes from the image resolution may lead to more realistic results.

Acknowledgments. This paper was supported by the Polish National Science Centre under grant no. 2013/08/M/ST7/00943.

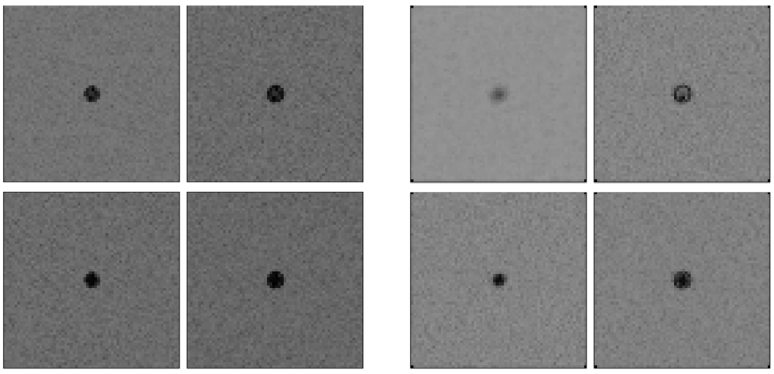

(A) (B)

Fig. 7. SWI images obtained with minimum intensity projection over 16 slices under 3 T main magnetic field using triangular mask with 0, 1, 4, 8 multiplications and noise of $\sigma = 1.2 \cdot 10^{-3}$ without (A) and with 3×3 median filter (B).

References

1. Haacke, E.M., Reichenbach, J.R., eds.: Susceptibility Weighted Imaging in MRI: basic Concepts and Clinical Applications. Wiley-Blackwell, New Jersey (2011)
2. Klepaczko, A., Kociński, M., Materka, A.: Quantitative description of 3d vascularity images: texture-based approach and its verification through cluster analysis. Pattern Analysis and Applications **14**(4) (2011) 415–424
3. Bittoun, J., Tacquin, J., Sauzade, M.: A computer algorithm for the simulation of any nuclear magnetic resonance (NMR) imaging method. J Magn Reson Imaging **3** (1984) 363–376
4. Kwan, R.S., Evans, A., Pike, G.: MRI simulation-based evaluation of image-processing and classification methods. Medical Imaging, IEEE Transactions on **18**(11) (1999) 1085–1097
5. Yoder, D.A., Zhao, Y., Paschal, C.B., Fitzpatric, J.M.: MRI simulator with object-specific field map calculations. Magnetic Resonance Imaging **22** (2004) 315–328
6. Benoit-Cattin, H., Collewet, G., Belaroussi, B., Saint-Jalmes, H., Odet, C.: The SIMRI project: a versatile and interactive MRI simulator. Journal of Magnetic Resonance **173** (2005) 97–115
7. Stoecker, T., Vahedipour, K., Pflugfelder, D., Shah, N.J.: High-performance computing mri simulations. Magnetic Resonance in Medicine **64**(1) (2010) 186–193
8. Klepaczko, A., Szczypiński, P., Dwojakowski, G., Strzelecki, M., Materka, A.: Computer simulation of magnetic resonance angiography imaging: Model description and validation. PLoS ONE **9**(4) (04 2014) e93689
9. Haacke, E.M., Brown, R.W., Thompson, M.R., Venkatesan, R.: Magnetic resonance imaging: physical principles and sequence design. Wiely-Loss, New York (1999)
10. Schenck, J.: The role of magnetic susceptibility in magnetic resonance imaging: MRI magnetic compatibility of the first and second kinds. Med. Phys. **23** (1996) 815–850
11. Liang, Z.P., Lauterbur, P.C.: Principles of Magnetic Resonance Imaging: A Signal Processing Perspective. IEEE Press, New York (2000)